High-Bandwidth Multiparametric Kelvin Probe Force Microscopy With Polymer Microcantilevers

HAO ZHANG [1], **XIANGHE MENG** [1], **JIANMIN SONG** [1], **JUNYUAN GENG** [1], **PENG JIN** [2], **AND HUI XIE** [1], **(Senior Member, IEEE)**

[1] State Key Laboratory of Robotics and Systems, Harbin Institute of Technology, Harbin 150080, China
[2] Center of Ultra-Precision Optoelectronic Instrument, Harbin Institute of Technology, Harbin 150080, China

Corresponding author: Hui Xie (xiehui@hit.edu.cn)

ABSTRACT Simultaneous and rapid measurement of the surface potential (SP) and nanomechanical properties (NMPs) of materials plays an important role in the study of, for example, piezoelectric materials and multi-component composites. In our previous study, a multiparametric Kelvin probe force microscopy (MP-KPFM) was developed to simultaneously measure SP and NMPs using traditional silicon probes. However, its temporal resolution is severely limited by the lower mechanical bandwidth of traditional silicon probes. Here, a composite atomic force microscope (AFM) probe capable of effectively increasing the measurement rate of MP-KPFM was developed. The proposed composite probe consisting of a polymer microcantilever and a silicon tip was fabricated using photolithography and microassembly techniques. Compared to the traditional silicon probe with a similar stiffness, its mechanical bandwidth is increased by about 4 times, which enables fast measurement by implementing the MP-KPFM at higher peak force drive frequencies. Experimental results show that the composite probe's peak force drive frequency is up to 4 kHz, whereas the traditional silicon probe is limited to about 1 kHz. Multiparametric mapping results of a polymer grating demonstrate the capability of the composite probe in fast and simultaneous measurement of SP and NMPs. The proposed composite probe has excellent compatibility and scalability due to the combination of the high mechanical bandwidth of the polymer microcantilever and the rigidity of the silicon tip, which provides a new idea for the development of multifunctional AFM probes.

INDEX TERMS Kelvin probe force microscopy, polymer microcantilever, high-bandwidth, surface potential, nanomechanical properties.

I. INTRODUCTION

Atomic force microscopy (AFM) [1] can achieve nano-scale resolution imaging of the surface potential (SP) [2]–[5] and nanomechanical properties (NMPs) [6]–[8]. It studies the properties of a sample by detecting the interaction between a nanoscale tip fixed on a cantilever and a sample [9]. Therefore, the force-sensing AFM probe plays an indispensable role which in charge of converting the tip-sample interaction into a voltage signal measured by a position sensitive detector (PSD) [10]. The quality factor of the AFM probe represents its response speed to oscillation and defines the

mechanical bandwidth of the AFM probe [11]. As the time resolution of the AFM continues to increase, the need to develop high-bandwidth AFM probes is becoming increasingly important.

The performance of the probe is not only related to the geometry of the cantilever, but also to the Young's modulus and the damping coefficient of the material used in the cantilever. Therefore, there are two main directions involved in the study to improve the mechanical bandwidth of the probe: (I) Optimizing the geometry of the cantilever, such as ultra-short probes [12], which are typically composed of materials with high Young's modulus and low damping coefficient [13], and are primarily used for high-speed topographical characterization in specific commercial AFM systems [14]–[16].

The associate editor coordinating the review of this manuscript and approving it for publication was Zhixiong Peter Li.

(II) Changing the material of the cantilever. Various materials with lower Young's modulus (<4 GPa) and larger damping coefficient, e.g. SU-8 photoresist [17], [18], have been proposed to fabricate AFM probes [17], [19]–[22], which can enable fast detection and characterization [23], [24] of fragile materials such as polymer semiconductors [25] or biological cells [26]. Therefore, polymer materials have become a new material for the preparation of fast-responding AFM probes [24], [27], [28]. However, when measuring the NMPs of a sample, in order to be able to ignore the deformation of the tip during the indentation, the Young's modulus of the probe tip is required to be much higher than that of the sample [29]. Thus, a polymer tip with low Young's modulus limits its measurable range of Young's modulus, making it primarily suitable for the measurement of soft materials.

To address the above-mentioned problems, a novel composite probe was proposed by assembling a silicon tip onto a polymer microcantilever, which inherits the advantages of high mechanical bandwidth of the polymer microcantilever and high hardness of the silicon tip. The performance of the proposed composite probe is significantly improved compared to traditional silicon probes. Its mechanical bandwidth is increased by about 4 times compared to a silicon cantilever of similar stiffness. In our previously developed multiparametric Kelvin probe force microscope (MP-KPFM) [30], the SP is measured during lifting of the probe. After the tip and sample are separated, the cantilever requires a certain decay time to transit to a steady state [24], [31], and the required decay time is inversely related to the mechanical bandwidth of the probe. The developed composite probe can significantly reduce the decay time and effectively improve the time resolution of the MP-KPFM. Experimental results show that the composite probe can rapidly and simultaneously characterize the SP and NMPs of materials with high Young's modulus ($E > 1$ GPa). This work will facilitate the application of AFM technology in the field of interface measurement.

The paper is organized as follows. Section II describes the experimental details, including the working principle of the MP-KPFM and the fabrication of the composite probe. The performance of the proposed composite probe is tested in Section III. Simultaneous measurement of SP and NMPs is performed in Section IV. Section V concludes this paper.

II. EXPERIMENTAL DETAILS
A. WORK PRINCIPLE OF THE MP-KPFM
As shown in Fig. 1, the mechanical drive signal of the probe for each measurement cycle in the MP-KPFM [30] consists of two parts: a peak force drive signal (Gaussian wave, much lower than the first-order resonant frequency of the probe, $f_{Gauss} \ll f_{1st}$) and a mechanical excitation with a small amplitude at its second-order resonant frequency (f_{2nd}). Each measurement cycle is divided into four working periods. Part A: the probe approaches the sample. Part B: the probe interacts with the sample. The NMPs of the sample are obtained at this stage. The snap-in point and pull-off point
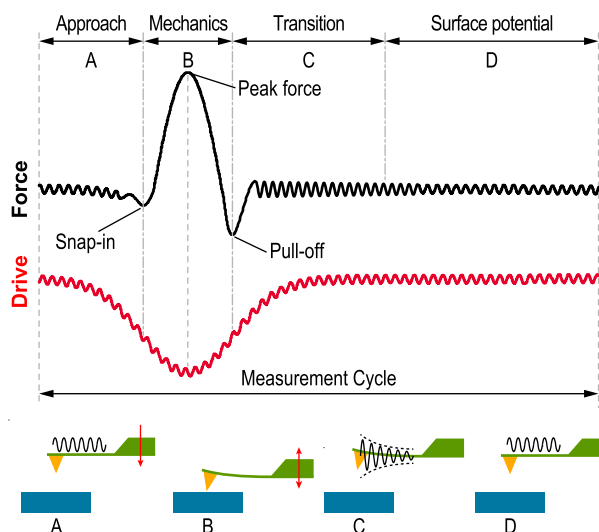

FIGURE 1. Top: the force feedback signal and mechanical drive signal of the probe during each measurement cycle of the MP-KPFM. Bottom: the schematic diagram of the working principle of the MP-KPFM.

are the initial contact point and the final detachment point of the probe and the sample, respectively. Part C: after the probe is detached from the sample, the free oscillation of the probe can be described by an exponential function. Part D: the probe maintains a stable mechanical oscillation at its second-order resonant frequency and the distance from the sample is constant (lift-up mode). At this stage, the SP of the sample is measured by using a direct current source (U_{DC}) to compensate for the contact potential difference (CPD) between the sample and the probe.

The time consumed in parts A and B is determined by the peak force drive frequency (f_{Gauss}), whereas the time consumed in part C is determined by the mechanical bandwidth of the probe. Therefore, the mechanical bandwidth of the probe limits the duration of the part D that can be used for SP measurement or the maximum frequency of the peak force signal (f_{Gauss}), in other words, the time resolution of the MP-KPFM. To increase the time resolution of the MP-KPFM, a microassembled composite probe is proposed, whose polymer microcantilever will significantly reduce the decay time of the probe (i.e., increase its mechanical bandwidth).

B. MICROASSEMBLY SYSTEM
As shown in Fig. 2, the proposed composite probe was fabricated on a high-precision micromanipulation system with a cantilevered micropipette probe (CMP) [32]. This system mainly consists of two optical microscopes (top view and side view), three holders, an AFM control system (an oscillation controller system, a PSD and a laser) and a pneumatic system (which enables positive and negative pressure switching at the CMP end, not shown here). During the manufacture of the composite probe, a CMP connected to the pneumatic system is mounted on a rotary holder with a piezo (holder I) to
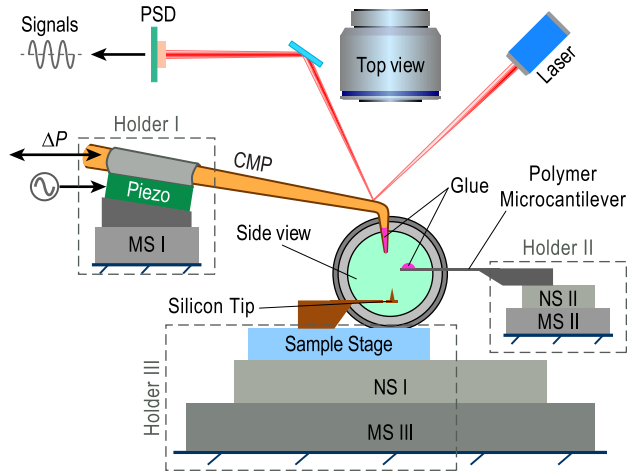
FIGURE 2. Schematic diagram of the high-precision micromanipulation system that can be used to assemble a composite probe.

FIGURE 3. SEM images of the polymer microcantilevers. Insets (a) and (b) are the side view and the zoom in of the polymer microcantilever E.

achieve absorption or deposition of the glue by adjusting the pressure (ΔP). The polymer microcantilever and the silicon tip are fixed on the holder II and the sample stage (holder III), respectively. Three micropositioning stages (MS-I, MS-II and MS-III) are used to move and align the CMP, the silicon tip and the polymer microcantilever, respectively. Two nanopositioning stages (NS I and NS II, providing subnanometer motion during assembly) precisely control the interaction between the polymer microcantilever and the CMP tip or the silicon tip based on the feedback signals acquired by the oscillation controller system. The more detailed descriptions can be found in our previous research [32].

C. FABRICATION OF THE COMPOSITE PROBE

The polymer microcantilevers required for the composite probe were fabricated using the SU8-Photoepoxy (GM1040, Gersteltec Sarl) by photolithography. The backside of the polymer microcantilevers has a vapor-deposited aluminum coating with thickness 300 nm to ensure the intensity of the reflective laser of the composite probe. The desired silicon tip was obtained by the focused ion beam technology to cut a traditional silicon probe (HQ: NSC36/Al-BS, MikroMasch). To obtain the polymer microcantilever with different stiffness, seven polymer microcantilevers with different lengths were designed, from 120 μm to 180 μm with a step of 10 μm. In addition, the width and thickness of the polymer microcantilever were designed to be 35 μm and 3 μm, respectively.

Fig. 3 is the scanning electron microscope (SEM) images of the polymer microcantilevers, which shows the physical dimensions of the polymer microcantilevers consistent with the initial design parameters. The decay time (τ) of the polymer microcantilever can be given as [11]:

$$\tau = \frac{2Q}{\omega} = \frac{Q}{\pi f} \qquad (1)$$

where Q and f are the quality factor and the resonant frequency of the polymer microcantilever, respectively.
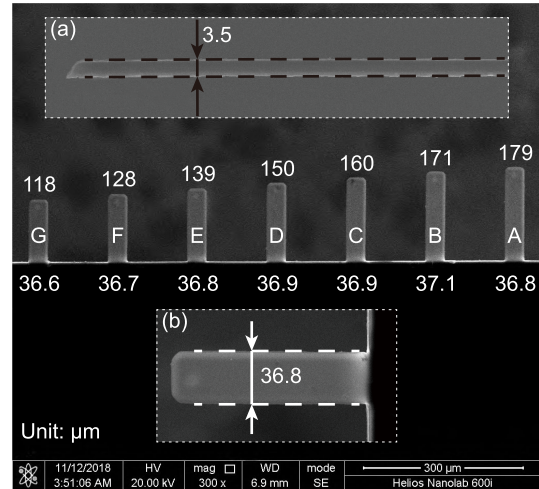
TABLE 1. Measurement results of the prepared polymer microcantilevers.

|	A	B	C	D	E	F	G
f_{1st}(kHz)	56.68	64.29	71.05	81.62	96.32	109.32	129.79
Q_{1st}	36	42	40	40	47	49	43
$1/\tau_{1st}$(kHz)	4.9	4.8	5.6	6.4	6.2	7.0	9.5
f_{2nd}(kHz)	368.76	377.11	455.38	511.95	605.11	673.59	801.45
Q_{2nd}	97	82	97	69	72	76	85
$1/\tau_{2nd}$(kHz)	11.9	14.4	14.7	23.3	26.4	27.8	29.6
k_{can}(N/m)	1.02	1.38	1.64	1.97	2.52	3.07	3.58

$\omega = 2\pi f$ is the angular frequency. The mechanical bandwidth of the polymer microcantilever is equal to the reciprocal of the decay time ($1/\tau$).

The stiffness (k) of the polymer microcantilevers can be calibrated by the Cleveland method [33]. In this method, k can be determined by:

$$k = (2\pi)^2 \frac{\Delta m}{1/(f_m - \Delta f_m)^2 - 1/f_m^2} \qquad (2)$$

where f_m is the first-order resonant frequency (f_{1st}) of the polymer microcantilever. Δf_m is the frequency shift of the first-order resonance frequency of the polymer microcantilever after adding a known mass (Δm), wherein a polystyrene (PS, $\rho = 1.05$ g/m^3) microbead with a diameter of 10 μm is used as the known mass in this paper.
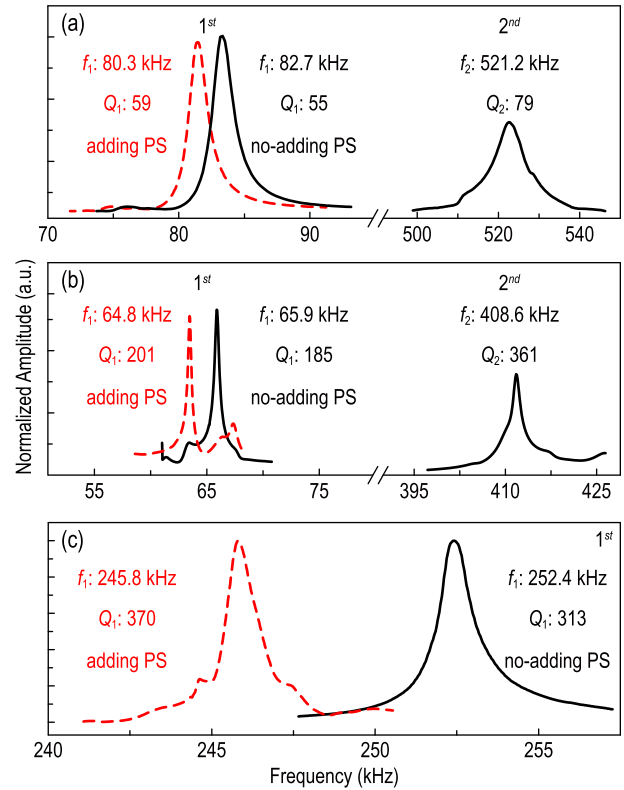
The measurement results of the polymer microcantilever prepared in this paper are shown in Table 1. The stiffness of the polymer microcantilevers vary from 1.02 to 3.58 N/m due to the different length of the microcantilevers. Their mechanical bandwidth also show a gradual trend (increasing as the stiffness increases, $1/\tau_{1st}$: from 4.8 to 9.5 kHz, $1/\tau_{2nd}$: from 11.9 to 29.6 kHz). The measurement results indicate the mechanical bandwidth of the polymer microcantilever is significantly improved even when the stiffness of the polymer microcantilever is smaller than that of a traditional silicon probe (HQ: NSC18/Al-BS: $k = 2.71$ N/m, $1/\tau_{1st} = 1.12$ kHz and $1/\tau_{2nd} = 3.55$ kHz, see the Fig. 5(b)), and prove that
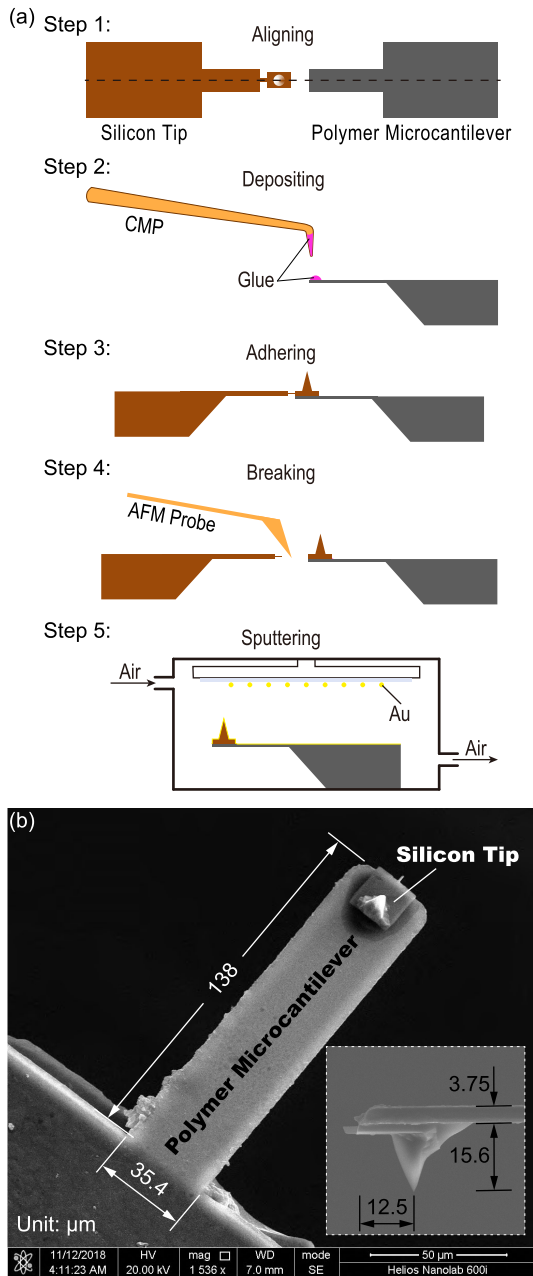
FIGURE 4. (a) Flow diagram for preparation of the composite probe: (Steps 1-4) assembling a silicon tip to a polymer microcantilever, (Step 5) sputtering a gold coating on the composite probe. (b) SEM images of the prepared composite probe. Inset is the side view of the tip of the composite probe.

FIGURE 5. Frequency responses of (a) the composite probe, (b) HQ: NSC18/Al-BS and (c) 160AC-NA, where the solid black line is the original resonance frequency of the probes, and the red dashed line is the first-order resonance frequency of the probe after adding a PS microbead.

polymer microcantilever were aligned. Then, the glue (epoxy adhesive, A-05HP, Angeluo, lap shear strength: 18 N/mm^2) was deposited to the front end of the polymer microcantilever by the CMP. Next, the silicon tip was adhered to the polymer microcantilever. After 20 minutes, the slender neck of the silicon tip was broken using a tip-visible probe (AETC-NC, Nanosensors) to separate the tip from its native cantilever. Finally, a gold coating was sputtered on the composite probe by the magnetron sputtering to ensure that the probe has excellent electrical conductivity. The SEM images of the prepared composite probe are shown in Fig. 4(b), which shows that the length, width and thickness of the polymer microcantilever are 138 μm, 35.4 μm and 3.75 μm, respectively. The tip height and setback are 15.6 μm and 12.5 μm.

III. PERFORMANCE TESTS OF THE COMPOSITE PROBE

To verify the performance of the composite probe, the test results of the composite probe were compared with those of two traditional silicon probes. One probe is similar in stiffness (HQ: NSC18/Al-BS, MikroMasch) and the other is similar in geometry (160AC-NA, MikroMasch). Fig. 5 shows the resonant frequency of the three probes, where the solid black line is the measurement before adding mass and the red dashed line is the measurement after adding mass.

As shown in Table 2, the performance parameters of three probes can then be obtained according to Eq. (1) and Eq. (2).

the polymer microcantilever prepared by photolithography has a flexible stiffness and excellent dynamic characteristics, which facilitate the popular use of the polymer microcantilever. The difference between the first-order and second-order mechanical bandwidths of the same microcantilever is mainly due to the increase of the damping of the air and the microcantilever as the vibration frequency of the microcantilever increases [34].

Fig. 4(a) shows the flow of assembling a silicon tip onto a polymer microcantilever. Firstly, the silicon tip and the

TABLE 2. Performance parameters of three AFM probes.

	$1/\tau_{1st}$ (kHz)	$1/\tau_{2nd}$ (kHz)	k (N/m)
The composite probe	4.72	20.70	2.50
HQ: NSC18/Al-BS	1.12	3.55	2.71
160AC-NA	2.53	—	25.4
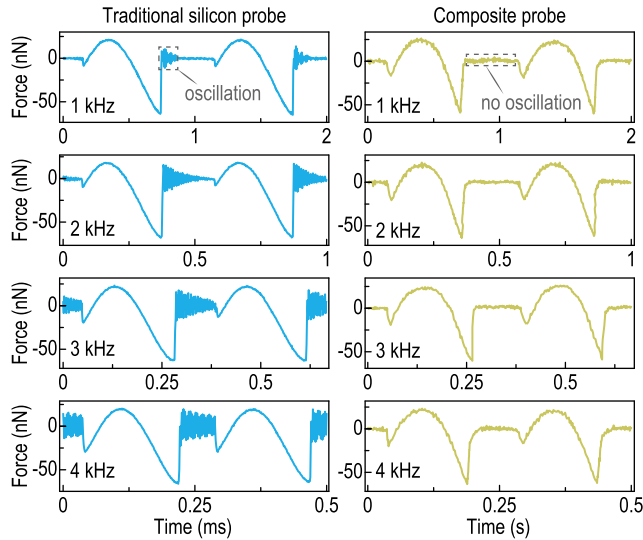
FIGURE 6. The force feedback signals of the traditional silicon probe (HQ: NSC18/Al-BS) and the composite probe. The peak force drive frequencies are 1, 2, 3 and 4 kHz, respectively.

The test result shows that the mechanical bandwidth of the composite probe is increased by about 4-5 times in the case of similar stiffness compared to the traditional silicon probe (HQ: NSC18/Al-BS). In addition, although the first-order resonant frequency of 160AC-NA is much higher than HQ: NSC18/Al-BS, its mechanical bandwidth (2.53 kHz) is not significantly improved. This slight improvement is mainly caused by an increase in the air damping due to an increase in the resonant frequency [34]. The above results indicate that in the case where the cantilever has the same shape, the mechanical bandwidth of the probe mainly depends on the material of the cantilever. Since the 160AC-NA probe has a stiffness of up to 25.4 N/m, it is not suitable for amplitude-modulation (AM)-KPFM mode in which MP-KPFM operates [35]. Therefore, the subsequent comparison was carried out between the traditional silicon probe (HQ: NSC18/Al-BS) and the composite probe.

Fig. 6 shows the force feedback signals for the traditional silicon probe and the composite probe with an adhesion of approximately 65 nN, which were obtained at four different peak force drive frequencies ($f_{Gauss} = 1, 2, 3$ and 4 kHz). Due to the presence of adhesion, the probe is vibrating after it separates from the sample. It can be seen from the results that the composite probe does not oscillate significantly after the probe is separated from the sample, regardless of whether the peak force drive frequency is 1 kHz or 4 kHz, which indicates that the consumption of the part C is short, that is, sufficient time is available for the SP measurement. For the traditional silicon probe, when the peak force drive frequency
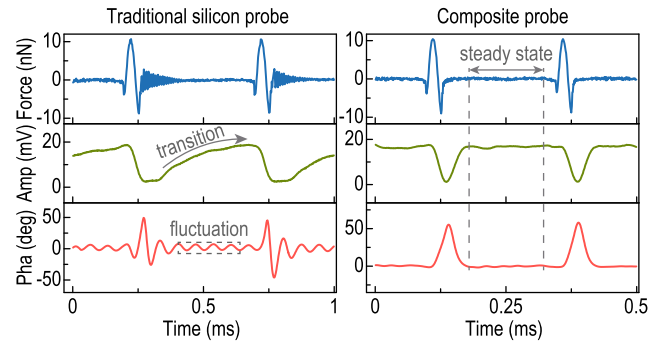
FIGURE 7. The force feedback signals, second-order amplitude and phase of the traditional silicon probe (HQ: NSC18/Al-BS, $f_{Gauss} = 2$ kHz) and the composite probe ($f_{Gauss} = 4$ kHz).

is 1 kHz, there is still adequate time to attenuate the oscillation of the probe, and there is a certain time for measuring the SP. However, when the peak force drive frequency is 2, 3 and 4 kHz, the time interval from the pull-off point to the next snap-in point is less than or equal to the time required by the part C. That is to say, the traditional silicon probe does not have enough part D for the SP measurement at the peak force drive frequencies of 2, 3 and 4 kHz. The above results indicate that when the SP and NMPs of the sample are simultaneously measured using the MP-KPFM method, the time resolution of the traditional silicon probe is even less than a quarter of the time resolution of the composite probe.

In the MP-KPFM, the second-order feedback signal of the probe is used to achieve the SP measurement of the sample. Fig. 7 shows the force feedback signals and the second-order amplitude & phase signals of two probes that were obtained at different peak force drive frequencies (HQ: NSC18/Al-BS: 2 kHz, Composite Probe: 4 kHz). It can be seen that the transition portion (Part C) is weakened due to low adhesion (<10 nN), but the second-order amplitude of the traditional silicon probe has a significant transition, and its phase signal also appears fluctuations. However, the second-order amplitude and phase of the composite probe remain approximately constant (in a steady state) after the probe is separated from the sample, which provides reliable feedback signals and sufficient time for the SP measurement. Since the relationship between the second-order phase of the probe and U_{DC} is monotonic, the phase feedback has better anti-interference ability than the amplitude feedback, so the second-order phase is selected as the feedback signal for the SP measurement in the MP-KPFM measurement [30], [36].

The above comparison results show that the composite probe has obvious advantages in performing MP-KPFM measurement compared to the traditional silicon probe. Its high-bandwidth feature can increase the time resolution of the MP-KPFM by about 4 times, and its silicon tip also has a wide Young's modulus measurement range ($E > 1$ GPa).

IV. RESULTS AND DISCUSSION
To demonstrate the superior performance of the composite probe described above, the prepared composite probe was

TABLE 3. Experimental parameters for performing the MP-KPFM with the composite probe.

	Gauss signal (f_{Gauss})	U_m	U_{AC}
Amplitude	60 nm	3 mV	4 V
Frequency	4 kHz	521.2 kHz	521.2 kHz

utilized to fast and simultaneously measure the SP and NMPs of a polymer grating sample at a high time resolution. The polymer grating sample was prepared by depositing the light curable adhesive (LCA, Loctite, 352) into a PS (Aladdin, CAS: 9003-53-6, P107085) trench prepared by soft lithography [37]. After the LCA was sufficiently dispersed into the PS trench, it was cured by irradiation with ultraviolet light (365 nm). The more detailed preparation process can be seen in previous research [30].

The experimental parameters used to perform the MP-KPFM using the prepared composite probe are described in Table 3, where the Gauss signal and U_m are the mechanical drive signals of the probe, and U_{AC} is a sinusoidal electric signal used to form an alternating electric field between the probe and the sample. In addition, the sample was connected to the positive electrode of U_{DC} in the experiment.

Fig. 8 shows the measurement results of the polymer grating using the composite probe. Fig. 8(a) is the topography of the polymer grating. As seen from the profile in Fig. 8(d), the height difference between the LCA and PS is from 60 nm to 150 nm. The adhesion mapping shown in Fig. 8(b) clearly shows that the PS and LCA have different surface characteristics under the same conditions. The statistical result shown in Fig. 8(e) displays that the adhesion between the PS/LCA and the gold-coated probe is 40.70 ± 9.48 nN (PS-Au) and 70.09 ± 9.26 nN (LCA-Au), respectively.

The reduced Young's modulus (E^*) of the polymer grating was calculated by the Derjaguin-Muller-Toporov model [38]:

$$F - F_{adh} = \frac{4}{3}E^*\sqrt{R\delta^3} \qquad (3)$$

where F is the force exerted by the probe on the sample, F_{adh} is the adhesion between the probe and the sample, R and δ are the tip apex radius and the indentation depth of the sample. Fig. 8(c) is the reduced Young's modulus imaging of the polymer grating, which clearly identifies the LCA and PS components. The bimodal fitting curve of the statistical distribution shown in Fig. 8(f) reveals the reduced Young's modulus results for the PS (2.05 ± 0.63 GPa) and LCA (0.45 ± 0.09 GPa), which is consistent with the mean Young's Modulus of the previous measurements [30], [39]. Compared with reference [30], the difference in standard deviation is mainly caused by the inherent nonuniformity of sample properties. It is almost impossible to measure the NMPs of materials with similar Young's modulus using polymer AFM tips. Due to the difference in Young's modulus of the sample, the deformation of the sample is also different when an equal force is applied to the sample. Fig. 8(g) is the deformation
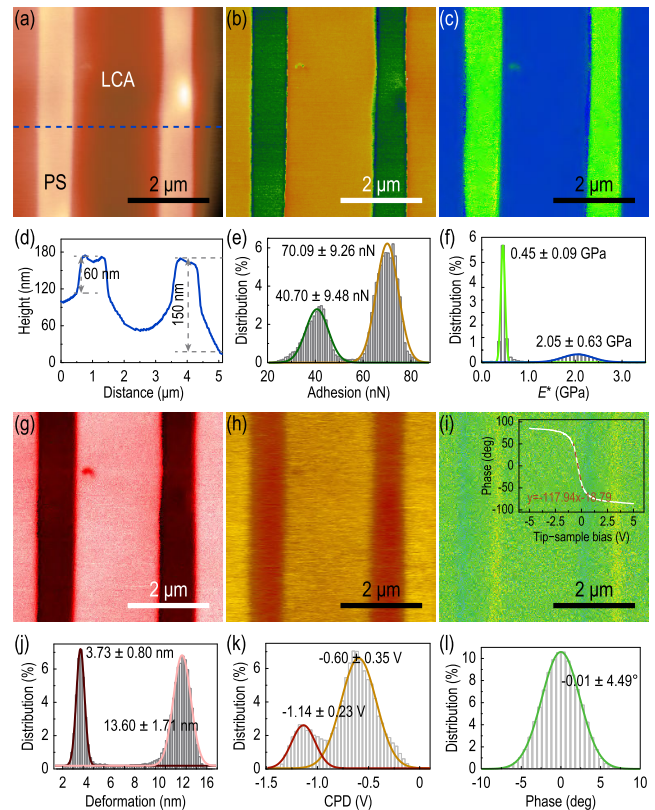
FIGURE 8. Imaging of topography (a), NMPs (b, c) and CPD (h) of the polymer grating by the microassembled composite probe. (g) and (i) are the deformation and phase in the experiment. The data below the images are the height profile and corresponding statistical distributions. Inset in (i) is the tip-sample bias (U_{DC}) vs phase curve calibrated before measuring the polymer grating. The linear fitting result (±50°) indicates a slope near zero phase of -117.94 deg/V.

mapping of the sample when the probe applies the maximum force to the sample ($F_{max} \cong 17$ nN). As can be seen from Fig. 8(j), the deformation of the PS and LCA are 3.73 ± 0.80 nm and 13.60 ± 1.71 nm, respectively.

As shown in Fig. 8(h), the CPD mapping also clearly distinguishes the difference in SP between the PS and LCA. Fig. 8(k) shows that the CPD between the polymer grating and Au-coated probe is -596.34 ± 345.41 mV (LCA) and -1136.78 ± 231.07 mV (PS), respectively. Considering that the sample was connected to the positive electrode of the U_{DC} in the experiment, the experimental results show that the SP of the PS is about 540 mV lower than the SP of the LCA. During the measurement of the SP, the phase was used as a feedback signal to eliminate the electric field force between the sample and the probe, keeping the phase equal to zero by adjusting the U_{DC}. Therefore, the offset of the phase with respect to the zero point represents the measurement error of the CPD. Fig. 8(i) and (l) show that the phase is basically consistent during SP measurement, with a average value of -0.01 °. The linear fitting result of the inset in Fig. 8(i) shows an absolute slope of 117.94 deg/V, which means that the average error is -0.08 mV.

V. CONCLUSION

In conclusion, a composite AFM probe consisting of a polymer cantilever and a silicon tip was developed. Compared with the traditional silicon probe in terms of dynamic performance, the mechanical bandwidth of the prepared composite probe is significantly improved by about 4 times, which effectively improves the measurement rate of AFM in quantification of surface properties of materials. Experimental results show that the proposed probe significantly improves the time resolution of the MP-KPFM in simultaneously measuring the surface potential and nanomechanical properties of materials. The probe with such a composite structure effectively solves the problem of low mechanical bandwidth of the traditional silicon probe and insufficient hardness of the polymer probe tip, and provides a new idea for developing multifunctional probes. It has great potential in optimizing the existing AFM methods and developing a new AFM methods.

REFERENCES

[1] G. Binnig, C. F. Quate, and C. Gerber, "Atomic force microscope," *Phys. Rev. Lett.*, vol. 56, no. 9, pp. 930–933, Mar. 1986.

[2] G. H. Enevoldsen, T. Glatzel, M. C. Christensen, J. V. Lauritsen, and F. Besenbacher, "Atomic scale Kelvin probe force microscopy studies of the surface potential variations on the TiO$_2$ (110) surface," *Phys. Rev. Lett.*, vol. 100, no. 23, Jun. 2008, Art. no. 236104.

[3] J. H. Lee, R. Hinchet, T. Y. Kim, H. Ryu, W. Seung, H. J. Yoon, and S. W. Kim, "Control of skin potential by triboelectrification with ferroelectric polymers," *Adv. Mater.*, vol. 27, no. 37, pp. 5553–5558, Oct. 2015.

[4] S. Li, Y. Zhou, Y. Zi, G. Zhang, and Z. L. Wang, "Excluding contact electrification in surface potential measurement using kelvin probe force microscopy," *ACS Nano*, vol. 10, no. 2, pp. 2528–2535, Feb. 2016.

[5] M. Persson, "Electric potentials at the atomic scale," *Nature Mater.*, vol. 18, no. 8, pp. 773–774, Aug. 2019.

[6] P. A. Fernandes, M. Delcea, A. G. Skirtach, and H. Möhwald, and A. Fery, "Quantification of release from microcapsules upon mechanical deformation with AFM," *Soft Matter*, vol. 6, no. 9, pp. 1879–1883, 2010.

[7] X. Meng, H. Zhang, J. Song, X. Fan, L. Sun, and H. Xie, "Broad modulus range nanomechanical mapping by magnetic-drive soft probes," *Nature Commun.*, vol. 8, Dec. 2017, Art. no. 1944.

[8] S. Benaglia, V. G. Gisbert, A. P. Perrino, C. A. Amo, and R. Garcia, "Fast and high-resolution mapping of elastic properties of biomolecules and polymers with bimodal AFM," *Nature Protocols*, vol. 13, no. 12, pp. 2890–2907, Dec. 2018.

[9] F. J. Giessibl, "Advances in atomic force microscopy," *Rev. Modern Phys.*, vol. 75, no. 3, pp. 949–983, Jul. 2003.

[10] Y. Seo and W. Jhe, "Atomic force microscopy and spectroscopy," *Rep. Prog. Phys.*, vol. 71, no. 1, Dec. 2007, Art. no. 016101.

[11] S. Morita, F. J. Giessibl, E. Meyer, and R. Wiesendanger, *Noncontact Atomic Force Microscopy*, vol. 3. Berlin, Germany: Springer, 2015.

[12] D. A. Walters, J. P. Cleveland, N. H. Thomson, P. K. Hansma, M. A. Wendman, G. Gurley, and V. Elings, "Short cantilevers for atomic force microscopy," *Rev. Sci. Instrum.*, vol. 67, no. 10, pp. 3583–3590, Nov. 1996.

[13] S. Akamine, R. C. Barrett, and C. F. Quate, "Improved atomic force microscope images using microcantilevers with sharp tips," *Appl. Phys. Lett.*, vol. 57, no. 3, pp. 316–318, Jul. 1990.

[14] P. K. Hansma, G. Schitter, G. E. Fantner, and C. Prater, "Applied physics: High-speed atomic force microscopy," *Science*, vol. 314, no. 5799, pp. 601–602, Oct. 2006.

[15] N. Kodera, D. Yamamoto, R. Ishikawa, and T. Ando, "Video imaging of walking myosin V by high-speed atomic force microscopy," *Nature*, vol. 468, no. 7320, pp. 72–76, Nov. 2010.

[16] H. S. Liao, C. W. Yang, H. C. Ko, E. T. Hwu, and S. Hwang, "Imaging initial formation processes of nanobubbles at the graphite-water interface through high-speed atomic force microscopy," *Appl. Surf. Sci.*, vol. 434, pp. 913–917, Mar. 2018.

[17] G. Genolet, J. Brugger, M. Despont, U. Drechsler, P. Vettiger, N. F. D. Rooij, and D. Anselmetti, "Soft, entirely photoplastic probes for scanning force microscopy," *Rev. Sci. Instrum.*, vol. 70, no. 5, pp. 2398–2401, May 1999.

[18] E. H. Conradie and D. F. Moore, "SU-8 thick photoresist processing as a functional material for MEMS applications," *J. Micromech. Microeng.*, vol. 12, no. 4, pp. 368–374, Jul. 2002.

[19] R. Pechmann, J. M. Kohler, W. Fritzsche, A. Schaper, and T. M. Jovin, "The novolever: A new cantilever for scanning force microscopy microfabricated from polymeric materials," *Rev. Sci. Instrum.*, vol. 65, no. 12, pp. 3702–3706, Dec. 1994.

[20] C. Ingrosso, C. Martin-Olmos, A. Llobera, C. Innocenti, C. Sangregorio, M. Striccoli, A. Agostiano, A. Voigt, G. Gruetzner, J. Brugger, F. Perez-Murano, and M. L. Curri, "Oxide nanocrystal based nanocomposites for fabricating photoplastic AFM probes," *Nanoscale*, vol. 3, no. 11, pp. 4632–4639, 2011.

[21] A. Gaitas and R. W. Hower, "SU-8 microcantilever with an aperture, fluidic channel, and sensing mechanisms for biological and other applications," *J. Micro/Nanolithogr.*, vol. 13, no. 3, Jul./Sep. 2014, Art. no. 030501.

[22] V. Martinez, P. Behr, U. Drechsler, J. Polesel-Maris, E. Potthoff, and J. Vörös, and T. Zambelli, "SU-8 hollow cantilevers for AFM cell adhesion studies," *J. Micromech. Microeng.*, vol. 26, no. 5, May 2016, Art. no. 055006.

[23] M. Calleja, M. Nordström, M. Álvarez, J. Tamayo, L. M. Lechuga, and A. Boisen, "Highly sensitive polymer-based cantilever-sensors for DNA detection," *Ultramicroscopy*, vol. 105, nos. 1–4, pp. 215–222, Nov. 2005.

[24] J. D. Adams, B. W. Erickson, J. Grossenbacher, J. Brugger, A. Nievergelt, and G. E. Fantner, "Harnessing the damping properties of materials for high-speed atomic force microscopy," *Nature Nanotechnol.*, vol. 11, no. 2, pp. 147–152, Feb. 2016.

[25] S. Keller, S. Mouaziz, G. Boero, and J. Brugger, "Microscopic four-point probe (u4PP) based on SU-8 cantilevers," in *Proc. Int. Conf. Micro- Nano Eng.*, 2005, Art. no. 125102.

[26] J. S. Lee, J. Song, S. O. Kim, S. Kim, W. Lee, J. A. Jackman, D. Kim, N. J. Cho, and J. Lee, "Multifunctional hydrogel nano-probes for atomic force microscopy," *Nature Commun.*, vol. 7, May 2016, Art. no. 11566.

[27] J. Mertz, O. Marti, and J. Mlynek, "Regulation of a microcantilever response by force feedback," *Appl. Phys. Lett.*, vol. 62, no. 19, pp. 2344–2346, May 1993.

[28] A. Boisen, S. Dohn, S. S. Keller, S. Schmid, and M. Tenje, "Cantilever-like micromechanical sensors," *Rep. Prog. Phys.*, vol. 74, no. 3, May 2011, Art. no. 036101.

[29] B. Pittenger, N. Erina, and C. Su, "Quantitative mechanical property mapping at the nanoscale with peakforce QNM," Bruker, Billerica, MA, USA, Appl. Note 128, 2010, pp. 1–12.

[30] H. Xie, H. Zhang, D. Hussain, X. Meng, J. Song, and L. Sun, "Multi-parametric Kelvin probe force microscopy for the simultaneous mapping of surface potential and nanomechanical properties," *Langmuir*, vol. 33, no. 11, pp. 2725–2733, Mar. 2017.

[31] L. Collins, M. Ahmadi, T. Wu, B. Hu, S. V. Kalinin, and S. Jesse, "Breaking the time barrier in Kelvin probe force microscopy: Fast free force reconstruction using the G-mode platform," *ACS Nano*, vol. 11, no. 9, pp. 8717–8729, Sep. 2017.

[32] H. Xie, H. Zhang, J. Song, X. Meng, Y. Wen, and L. Sun, "High-precision automated micromanipulation and adhesive microbonding with cantilevered micropipette probes in the dynamic probing mode," *IEEE/ASME Trans. Mechatronics*, vol. 23, no. 3, pp. 1425–1435, Jun. 2018.

[33] J. Cleveland, S. Manne, D. Bocek, and P. Hansma, "A nondestructive method for determining the spring constant of cantilevers for scanning force microscopy," *Rev. Sci. Instrum.*, vol. 64, no. 2, pp. 403–405, Feb. 1993.

[34] T. Glatzel, S. Sadewasser, and M. C. Lux-Steiner, "Amplitude or frequency modulation-detection in Kelvin probe force microscopy," *Appl. Surf. Sci.*, vol. 210, nos. 1–2, pp. 84–89, Mar. 2003.

[35] U. Zerweck, C. Loppacher, T. Otto, and S. Grafström, and L. M. Eng, "Accuracy and resolution limits of Kelvin probe force microscopy," *Phys. Rev. B, Condens. Matter*, vol. 71, no. 12, Mar. 2005, Art. no. 125424.

[36] D. Ziegler, J. Rychen, N. Naujoks, and A. Stemmer, "Compensating electrostatic forces by single-scan Kelvin probe force microscopy," *Nanotechnology*, vol. 18, no. 22, Jun. 2007, Art. no. 225505.

[37] M. A. Unger, H. P. Chou, T. Thorsen, A. Scherer, and S. R. Quake, "Monolithic microfabricated valves and pumps by multilayer soft lithography," *Science*, vol. 288, no. 5463, pp. 113–116, Apr. 2013.

[38] J. Adamcik, C. Lara, I. Usov, J. S. Jeong, F. S. Ruggeri, G. Dietler, H. A. Lashuel, W. Hamley, and R. Mezzenga, "Measurement of intrinsic properties of amyloid fibrils by the peak force QNM method," *Nanoscale*, vol. 4, no. 15, pp. 4426–4429, 2012.

[39] E. T. Herruzo, A. P. Perrino, and R. Garcia, "Fast nanomechanical spectroscopy of soft matter," *Nature Commun.*, vol. 5, Jan. 2014, Art. no. 3126.

JUNYUAN GENG received the B.S. degree in mechanical engineering from Yanshan University, Qinhuangdao, China, in 2017, where she is currently pursuing the Ph.D. degree with the State Key Laboratory of Robotics and Systems.

Her main research interest includes surface charge mapping with atomic force microscope.
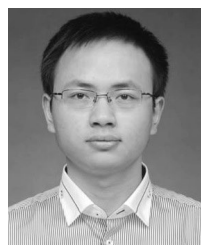
HAO ZHANG received the B.S. degree in mechanical engineering and automation from the Kunming University of Science and Technology, Kunming, China, in 2013, and the M.S. and Ph.D. degrees in mechatronics engineering from the Harbin Institute of Technology, Harbin, China, in 2015 and 2019, respectively.

His research interests include multiparametric imaging and characterization at micro/nano interfaces using atomic force microscope/Kelvin probe force microscope, and micro- and nano-manipulation with the micro- and nano-robotic systems.

PENG JIN received the Ph.D. degree in instrument science and technology from the Harbin Institute of Technology, Harbin, China, in 2001.

He is currently a Professor with the Center of Ultra-Precision Optoelectronic Instrument, Harbin Institute of Technology, and is also an Honorary Associate Professor with the University of New South Wales. His research focuses on nanoimprinting, fabrication, and application of micro-optics elements.

XIANGHE MENG received the B.S. degree in mechatronics engineering from the Harbin Institute of Technology, Harbin, China, in 2014, where he is currently pursuing the Ph.D. degree in mechanical engineering.

His research interests include nanomechanics at the micro- and nano-surfaces/interfaces and robotic micro- and nano-manipulation.

HUI XIE received the Ph.D. degree in mechatronics engineering from the Harbin Institute of Technology, Harbin, China, in 2006.

He was a Research Associate with the Institut des Systèmes Intelligents et Robotique, Université Pierre et Marie Curie/Centre National de la Recherche Scientifique, Paris, France, from 2008 to 2010, where he was also a Postdoctoral Researcher, from 2006 to 2008. He is currently a Full Professor with the State Key Laboratory of Robotics and Systems, Harbin Institute of Technology. His current research interests include micro- and nano-robotics, nanomanipulation/characterization, AFM three-dimensional micro- and nano-CD metrology, AFM multiparametric imaging and characterization of complex cellular and biomolecular systems under physiological conditions, and micro- and nano-swimming robots.

JIANMIN SONG received the M.S. degree in mechanical engineering from the Harbin Institute of Technology, Harbin, China, in 2015, where he is currently pursuing the Ph.D. degree in mechanical engineering with the State Key Laboratory of Robotics and Systems.

His main research interests include scanning ion conductive microscope imaging and applications on biological cell characterization.

● ● ●